Orally Fast Dissolving *α*-Lipoic acid Electrospun Nanofibers Mitigates Lipopolysaccharide Induced Inflammation in RAW 264.7 Macrophages

1. Introduction

In recent years, Oral Thin Films (OTFs) have emerged as a potential approach for nutraceutical delivery especially for paediatrics and geriatrics. These formulations can overcome certain technological challenges in nutraceutical delivery such as chemical instability in gastro-intestinal tract, low aqueous solubility, low permeability, chemical degradation, hepatic – first pass metabolism, and efflux transporter specificity. Further, a recent clinical study (on 50 healthy volunteers) demonstrated electrospinning method to be a preferred choice as compared to solvent casting method in terms of sensory attributes of end-user acceptability, which renders them suitable for clinical translation.

Current work highlights the significance of combined effect of inclusion complexation and nanofiber technology as a potential rapid disintegrating delivery system for α-lipoic acid (a dietary supplement). Lipoic acid (LA) is a dietary supplement with a double-sulfhydryl structure that acts as a cofactor for enzymatic complexes involved in cellular energy production[1, 2]. LA exhibits antioxidant and anti-inflammatory characteristics, with its antioxidant effects being linked to the enhanced functioning of antioxidant enzymes like glutathione reductase, reinstatement of the equilibrium between reduced and oxidized glutathione, and decrease in $NADP^+$ levels[3]. Inflammation and oxidative stress are common features observed in various pathological conditions like diabetic polyneuropathy and Alzheimer's disease. These conditions are characterized by the activation of inflammatory pathways, leading to an overproduction of nitric oxide (NO) and reactive oxygen species (ROS)[4]. A recent clinical study also demonstrated that a four-month treatment with LA in patients with type 2 diabetes mellitus led to significant reductions in inflammatory markers. Specifically, C-reactive protein (CRP) levels were reduced by 30.9%, interleukin-6 (IL-6) by 29.7%, and tumor necrosis factor-alpha (TNF-α) by 22.7 %[5]. The exceptional therapeutic potential of LA is limited by certain technological challenges including low aqueous solubility and susceptibility to heat-induced degradation [2]. To address these issues, we have utilized methyl-beta-cyclodextrin (M-*β*-CD) to create inclusion complex (IC) of LA and thereafter encapsulated in pullulan nanofiber using green and sustainable approach (without utilizing organic solvent). The developed

nanofibers (NF) demonstrated accelerated release, quick dissolution, and disintegration along with high encapsulation efficiency. Additionally, NF demonstrated the ability to downregulate the production of NO, ROS, suppresses the upregulation of pro-inflammatory enzymes (iNOS and COX-2), cytokines (TNF-α, IL-6, and IL-1*β*) and nuclear translocation of NF-κB in lipopolysaccharide (LPS) stimulated RAW 264.7 macrophage cells. The study has opened new avenues in terms of sustainable approach for production of nanofibers as well as its mechanistic insight for anti-inflammatory activity.

2. Objectives

The objectives of the study were:

1. Development of patient friendly and convenient electrospun oral thin film of lipoic acid (a dietary supplement).

2. Characterization and critical quality attribute (CQA) evaluation of developed nanofiber film.

3. Cytocompatibility evaluation and mechanistic insight of nanofiber film against LPS induced inflammation in RAW 264.7 macrophages.

3. Material and Methods

Matrix assisted laser desorption ionisation/time-of-flight mass spectrometry (MALDI-TOF)

The MALDI-TOF-TOF mass spectrometer (Bruker ultra TOF, USA) was used to determine the average molecular weight of the cyclodextrins (M-*β*-CD and HP-*β*-CD). Prior to analysis, 1 µL of CD solution was applied to a metal plate, followed by 1 µL of saturated solution containing α-Cyano-4-hydroxycinnamic acid (CHCA) matrix. In positive ion reflector mode, spectra were captured in the mass range of 700-3500 Da. Flex Analysis software was used to examine the acquired data [6].

Phase solubility

The solubility of LA was analyzed using the Higuchi and Conners method [7]. In this experiment, different concentrations (0-12 mM) of *β*-CD, M-*β*-CD and HP-*β*-CD in water were prepared in 2 mL microcentrifuge tubes. Thereafter, an excess amount of

LA was added in each tube and incubated at 25°C for 24 h in IKA® matrix orbital shaker (Delta F2.0, Germany) [8]. After 24 h, the suspensions were centrifuged at 10,000 rpm for 10 minutes and filtered to remove any undissolved LA. The extent of LA solubility was analysed using isocratic method with binary elution system of methanol: 0.01% TFA water (70:30) at 335 nm wavelength *via* HPLC (Agilent 1260 Inifinity II). The average of three measurements was used to plot the phase solubility graph and fold increase in solubility. The binding constant (Ks) was calculated using the following equation.

$$Ks = \frac{Slope}{S_{\circ}(1 - Slope)}$$

Where, $S_{\circ}$ is the solubility of LA in water/without CD. Slope can be derived from the linear equation of phase solubility curve.

Development of lipoic acid/cyclodextrin inclusion complex pullulan nanofiber

The inclusion complex of LA with M-*β*-CD was prepared by mixing them in 1:1 molar ratio (LA: M-*β*-CD). Initially, M-*β*-CD (23 % w/v) was dissolved in water followed by the addition of LA [9]. The mixture was incubated overnight at room temperature (RT) with continuous stirring, resulting in a clear solution of the inclusion complex. Further, pullulan (20 % w/v) was incorporated in the LA-M-*β*-CD inclusion complex and stirred at RT to get clear solution. The conductivity and viscosity of the solution was also measured using a conductivity meter (deluxe conductivity meter, Model-602) and (viscometer, IKA ROTAVISC lo-vi) respectively. The developed solution was filled in 1 mL syringes with stainless-steel needle (27 G) placed horizontally and was subjected for electrospinning (E-SPIN NANOTECH, model: Super ES-1) at high voltage (15 kV) with constant flow rate of 0.5 mL/h [8]. The blank nanofibers consisting of pure pullulan and cyclodextrin solutions without LA was also prepared using the same protocol.

Characterization and Critical quality attribute evaluation of nanofibers

Morphological and structural characterization

The morphology of the developed NFs was investigated using Scanning electron microscopy (SEM, model S-3400N, Hitachi, Tokyo, Japan). The average diameter (AD, mean ± SD) of NFs was determined using ImageJ software based on at least

100 measurements, from different locations of micrographs. The developed NFs were checked for the presence of their chemical structure composition using proton nuclear magnetic resonance (^{1}H NMR) spectroscopy. The chemical shifts (δ) values were plotted in parts per million (ppm) relative to the TMS signal (0 ppm). The Fourier transform infrared (FT-IR) spectra of native LA, PUL, M-*β*-CD, and PUL/LA/M-*β*-CD NF were recorded in the range of 4000–550 cm^{-1} (PerkinElmer, ES version 10.5.3 software). The thermal behaviour of LA, PUL, M-*β*-CD, and PUL/LA/M-*β*-CD NF were analysed by differential scanning calorimeter (DSC, DSC200, Hitachi). Prior to analysis, the 3-5 mg of samples were sealed in chromated aluminum pan and heated from 25°C to 250°C at a scanning rate of 10 °C/min under a dry nitrogen flow (flow rate: 50 mL/min). An empty sealed chromated aluminum pan was used as reference. Further, the thermal degradation behaviour of LA, PUL, M-*β*-CD, and PUL/LA/M-*β*-CD NF was recorded using thermogravimetric analyzer (TGA, Mettler Toledo, model: TGA/DSC-I, Columbus, OH, USA). The diffraction patterns of LA, PUL, M-*β*-CD, and the PUL/LA/M-*β*-CD NF were recorded using powder X-ray diffractometer (Rigaku Corporation, Tokyo, Japan).

Time dependent release of LA

The release profile of PUL/LA/M-*β*-CD NF was investigated using phosphate-buffered saline (PBS) solution for 12 minutes. Initially, the NF sample was weighed (equivalent to 10 mg of LA), dissolved in PBS solution and placed on magnetic stirrer at a 200 rpm speed. The aliquots of 0.7 mL were withdrawn from the solution at specific time intervals (0, 60, 120 seconds, up to 720 seconds) and solution was replenished with an equal volume of fresh PBS [8]. The dissolved LA content in the samples were analysed using high-performance liquid chromatography (HPLC). The release test was conducted in triplicate, and the results are reported as the mean ± SD.

***In vitro* dissolution and disintegration**

The dissolution test was conducted with LA, PUL/LA/M-*β*-CD NF and blank NF. The samples were placed in glass vials and 5 mL of distilled water was added to each vial while video recording to observe the dissolution process. The disintegration behaviour of PUL/LA/M-*β*-CD NF and the blank NF were examined in a simulated physiological environment resembling the moist surface of tongue. In brief, a filter

paper of appropriate size was positioned in a petri dish and moistened with artificial saliva. The artificial saliva was developed using 1.4 mM KH_2PO_4, 16.8 mM Na_2HPO_4, 137 mM NaCl in10 mL of an aqueous solution with the pH 6.8 [8]. After removing extra synthetic saliva from the petri dish, a piece of PUL/LA/M- *β*- CD NF or blank NF was positioned in the middle of the filter paper and disintegration processes were captured.

Cell culture

RAW 264.7 murine macrophages were obtained from the National Centre for Cell Science (NCCS), Pune, India. The cells were revived and cultivated using DMEM media with 10% foetal bovine serum (FBS, Gibco, USA) and 1% antibiotic–antimycotic solution. The cultures were kept at 37°C with 5 % CO_2 atmosphere in incubator. Further, cells were treated with LA and PUL/LA/M- *β*- CD NF at different concentrations (100 µM, 250 µM, and 500 µM equivalent to LA) for 24 h followed by LPS (1 µg/mL) induction for another 24 h.

***In vitro* evaluation of anti-inflammatory potential of nanofibers**

Cell viability assay

The inhibitory effect of PUL/LA/M-*β*-CD NF on the growth of RAW 264.7 cells with or without LPS induction was assessed using MTT assay[10]. Briefly, cells were cultivated in 96-well plates at a density of 1×10^4 cells per well and treated with different concentrations of LA and PUL/LA/M-*β*-CD NF followed by LPS induction for 24 h. After LPS induction, MTT solution was added to each well and incubated for an additional 4 h at 37°C. The formazan crystals were dissolved with DMSO after complete removal of culture media and optical density at 570 nm was measured by microplate reader (Infinite® 200 PRO from Tecan)***.*** The morphological changes of macrophages after LPS induction and NF treatment were captured using fluorescent cell imager (ZOE™ Fluorescent Cell Imager, Bio-Rad). Percent cell viability was calculated by using following equation:

$$\%\ Cell\ Viability = \frac{OD_{test}}{OD_{control}} * 100$$

NO production estimation by griess reagent

RAW 264.7 cells were seeded in a 96-well plate with 100 µL of cell suspension containing 1 × 10^6 cells per well. The cells were pre-treated with different concentrations of LA and PUL/LA/M-β-CD NF and incubated at 37 °C for 24 h. After the pre-treatment, the cells were exposed to LPS (1 µg/mL) for 24 h for the production of nitric oxide (NO). After the incubation, 100 µL of the supernatant from each well was collected and equal volume of the Griess reagent was added for NO estimation. Finally, absorbance was measured at 535 nm using microplate reader (Infinite® 200 PRO, Tecan, USA) [11]. The standard curve was prepared using sodium nitrite to calculate the amount of NO production.

Reactive oxygen species analysis

The effect of PUL/LA/M-*β*-CD NF on LPS induced ROS generation in RAW 264.7 macrophages was analysed by using carboxy-2,7-dichlorohydrofluorescein diacetate (DCF-DA) dye. After treatment of LA and PUL/LA/M-*β*-CD NF for 24 h at different concentrations, followed by LPS induction, the adherent cells were washed with PBS and incubated with carboxy-2,7-dichlorohydrofluorescein diacetate (DCF-DA constituted in PBS, 100 µL) for 30 minutes at 37 °C [12]. Thereafter, the cells were re-washed with PBS and images were captured using fluorescent microscope (EVOS FL Auto 2 Cell Imaging System, Invitrogen). The quantification of ROS was performed using microplate spectrophotometer (Synergy-H1, hybrid reader, BioTek® 275) by measuring the fluorescence intensity at 488 nm (excitation) and 535 nm (emission).

qRT-PCR of pro-inflammatory enzyme and cytokine genes

RAW 264.7 macrophages were plated in a 6-well plate with 1 mL of cell suspension containing 1 × 10^6 cells per well. The cells were treated with LA and PUL/LA/M-*β*-CD NF for 24 h followed by LPS induction for another 24 h at 37 °C. Total RNA isolation was performed by using TRIzol reagent (Ambion, Life technologies) and chloroform. The concentration and purity of RNA was assessed by nanodrop quantification using NanoDrop™ One/OneC Microvolume UV-Vis Spectrophotometer (Thermo Fisher Scientific, MA, USA). Verso 1-step RT-qPCR Kit with SYBR Green and ROX and CFX Opus Real-Time PCR Systems was used for qRT-PCR of targeted genes. Specific primers for the targeted genes, including COX-2, iNOS, IL-6, IL-1*β*, TNF-*α*,

and *β*-actin were used for PCR amplification of the cDNA. The relative mRNA expressions were quantified using $2^{-\Delta\Delta Ct}$ method and *β*-actin was used as housekeeping gene to normalize the mRNA expression. The primer sequences of *β*-actin, IL-1*β*, TNF-*α*, IL-6, iNOS and COX-2 was constructed by Primer express software.

Western blot of primary pro-inflammatory enzyme: COX-2

The pro-inflammatory enzyme, COX-2 protein expression was analysed by western botting. Briefly, RAW 264.7 macrophages were seeded in a six-well plate with 1 mL of media per well, containing 1×10^6 cells. Cells were treated with LA and PUL/LA/M-*β*-CD nanofiber solution for 24 h, followed by LPS induction for another 24 h at 37 °C. Following incubation, the cells were collected, washed twice with cold PBS and lysed with RIPA buffer and PIC. The cell lysates were freeze thawed for protein extraction which were further collected and centrifuged at 14,000 rpm for 10 minutes at 4 °C. The Bradford assay was used to calculate the protein concentrations [13].

The extracted proteins (30 µg/lane) were fractionated by 10 % SDS-PAGE gel, transferred to PVDF membrane using semi-dry trans-blotter system. The blots were incubated with primary antibodies, specifically anti-COX-2 (Cell Signalling Technology Inc., Beverly, MA, USA) and anti-*β*-actin (Elabscience), overnight at 4 °C. After incubation, membrane was washed with TBST and incubated with a secondary antibody, an anti-rabbit IgG HRP conjugated antibody. After washing with 1x TBST, the protein bands were visualized using an enhanced chemiluminescence (ECL) substrate and image was captured using Azure c300 Gel imager. The bands were quantified using ImageJ software and normalised by the bands of *β*-actin.

NF-κB protein translocation assay

The effect of PUL/LA/M-*β*-CD NF on nuclear localization of NF-κB was examined through immunofluorescence staining. Macrophages were exposed with LA and PUL/LA/M-*β*-CD NF for 12 h followed by LPS induction for 6 h. After washing with PBS, cells were fixed with 4% paraformaldehyde (40 min. at RT) and permeabilized with 0.25% Triton X-100 (20 min. at RT). Afterwards, the cells were incubated in blocking solution (5% BSA) for 1 h and treated with primary antibody (anti-NF-κ-B-p65 antibody, L8F6, Cell Signalling Technology Inc., Beverly, MA, USA) at a dilution

of 1:800. A secondary antibody labelled with Alexa Fluor 488 (Cell Signalling Technology Inc., Beverly, MA, USA), particularly directed against anti-mouse IgGk, was used to visualize the translocation of NF-κB [11]. The nuclei were stained with DAPI (2 µg/mL) for 10 minutes. Following another round of PBS washing, images were captured using fluorescence microscope (EVOS FL Auto 2 Cell Imaging System, Invitrogen).

4. Results and Discussion

Mass spectra of M-*β*-CD and HP-*β*-CD

The mass spectra of both M-*β*-CD as well as HP-*β*-CD was recorded to determine the degree of substitution and average molecular weight before conducting phase solubility of LA with CD derivatives. MALDI spectra of M-*β*-CD demonstrated peak difference of 15 Da corresponding to the molecular weight of one methyl substitution with average molecular weight of 1302.764 Da. Likewise, MALDI spectra of HP-*β*-CD demonstrated peak difference of 58 Da corresponding to the molecular weight of one hydroxypropyl substitution and average molecular weight of 1482.789 Da. From the MALDI spectra of both CDs (M-*β*-CD and HP-*β*-CD) and molecular weight of *β*-CD (1135 g/mol), this can be inferred that degree of substitution lies in between 8-16 for M-*β*-CD and 2-9 for HP-*β*-CD. The observed average molecular weight of both M-*β*-CD and HP-*β*-CD were in correlation with the previously conducted mass studies [6, 14].

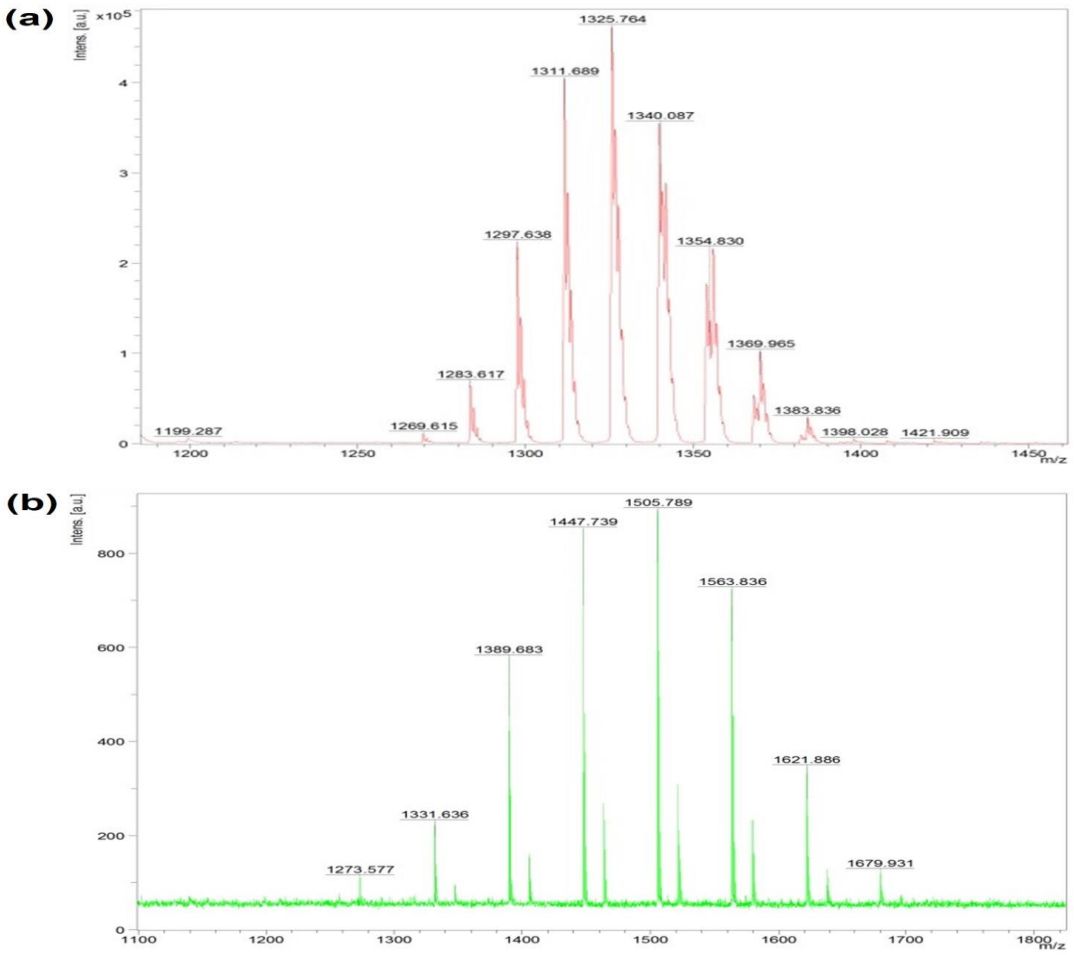

Figure 1: Mass spectrum of (a) Methyl-*β*-cyclodextrin (M-*β*-CD) and (b) Hydroxypropyl- *β*-cyclodextrin (HP-*β*-CD). In spectra of M-*β*-CD, substitution number of methyl moiety demonstrated by peak shifting in spectra of approximate mass unit (m/z) 15 Da which corresponds to the mass of one methyl moiety. In spectra of HP-*β*-CD, substitution number of hydroxypropyl moiety demonstrated by peak shifting in spectra of approximate mass unit (m/z) 58 Da corresponding to the mass of single hydroxypropyl moiety

Phase solubility studies: molar stoichiometric ratio and stability constant

The phase solubility studies of LA with *β*-CD, M-*β*-CD and HP-*β*-CD were conducted to determine the solubility, molar stoichiometric ratio, stability constant and to choose the best CD derivative for development of inclusion complex. The results of phase solubility revealed linear (A_L – type curve) increase in solubility of LA ranked in order M-*β*-CD (r^2 = 0.999) > HP-*β*-CD (r^2= 0.998)> *β*-CD (r^2 = 0.952), which represents 1:1 molar stoichiometric ratio (host: guest molecule) for all complexes as per Higuchi and Connors. Further, stability constant (K_S, M^{-1}) of inclusion complexes, which was calculated from slope of linear phase solubility plots, revealed highest value in case of M-*β*-CD (2523.8 M^{-1}) followed by HP-*β*-CD (1257.4 M^{-1}) and *β*-CD (717.4 M^{-1}).

The higher the value of stability constant usually indicates the higher stability and better ability of inclusion complex formation [15]. Therefore, on the basis of results M-*β*-CD was the preferable choice for inclusion complex formation with highest solubility and stability constant.

Electrospinning of nanofibers and morphological analysis

In this study, PUL/LA/M-*β*-CD NF was developed by using one-step electrospinning technique, which offers the advantage of incorporating higher concentrations of cyclodextrin leading to encapsulation/solubilisation of higher amount of bioactive molecules[9]. LA-M-*β*-CD inclusion complex was prepared by overnight incubation and then PUL (20% w/v) was directly added to the inclusion complex solution resulting in the formation of clear and homogenous system. The viscosity and conductivity plays crucial role in the development and morphology of nanofibers, therefore, both the parameters of electrospinning solution were recorded. The value of viscosity and conductivity of PUL/LA/M-*β*-CD NF solution was determined as 1332 ± 12 mPa.s and 1.28 ± 0.008 S/cm, respectively. One-step electrospinning technique imparts the advantage of enhanced encapsulation of inclusion complex inside PUL nanofibers with entrapment efficiency of ~ 86.90 %. The PUL/LA/M-*β*-CD NF was successfully developed from electrospinning solutions and demonstrated uniform, bead and defect free morphology with average nanofibers diameter of 569 ± 129 nm. This has been observed that low viscosity and high conductivity of the solution usually results in thinner fibres as compared to its counterparts[8, 9, 16]. The deviation of PUL/LA/M-*β*-CD NF size from blank nanofibers (127 ± 23 nm; 1229.3 ± 50.2 mPa.s) may be due to encapsulation of LA-M-*β*-CD inclusion complex as well as increase in viscosity of PUL/LA/M-*β*-CD solution (1332 ± 12 mPa.s.)

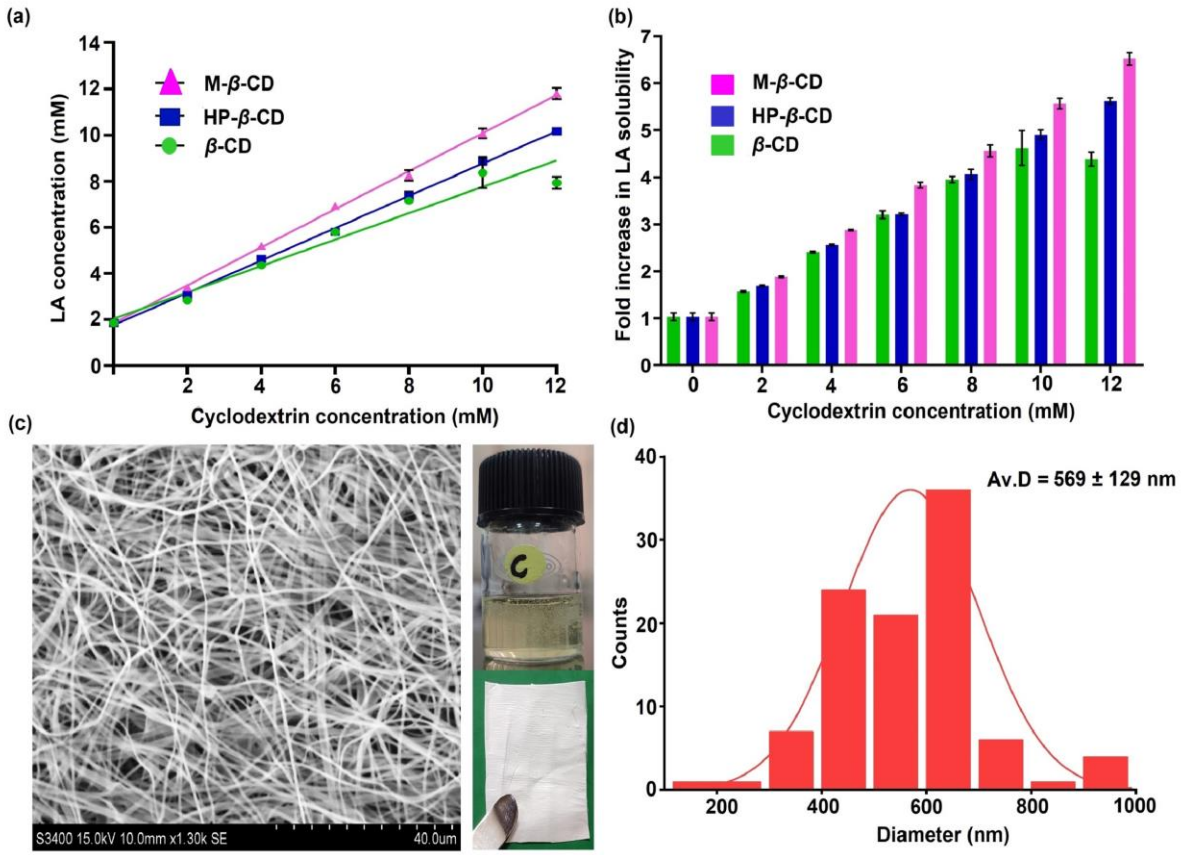

Figure 2: (a) Phase solubility curve and (b) fold increase in solubility of α-Lipoic acid (LA) with increasing molar concentration (0-12 mM) of *β*-CD (green colour); Hydroxypropyl- *β*-cyclodextrin (HP-*β*-CD; Navy blue colour) and Methyl-*β*-cyclodextrin (M-*β*-CD; magenta colour). (c) Scanning electron microscope image and (d) average fibre size distribution of PUL/LA/M-*β*-CD NF.

Structural characterization of PUL/LA/M-*β*-CD nanofiber

Nuclear magnetic resonance spectroscopy (NMR) analysis

The presence and successful encapsulation of LA within PUL/LA/M-*β*-CD nanofibers were analysed by ^{1}H-NMR spectra of LA, PUL, M-*β*-CD, and PUL/LA/M-*β*-CD individually. The distinctive peaks corresponding to the LA observed in the ^{1}H-NMR spectra of the nanofiber provided the evidence of LA being loaded into the PUL/LA/M-*β*-CD nanofibers [2]. Notably, the characteristic peaks of LA in the spectra of both LA and PUL/LA/M-*β*-CD nanofibers were identical, indicating the preservation of LA's chemical structure throughout the entire electrospinning process, thus ensuring its protection and stability [8, 9].

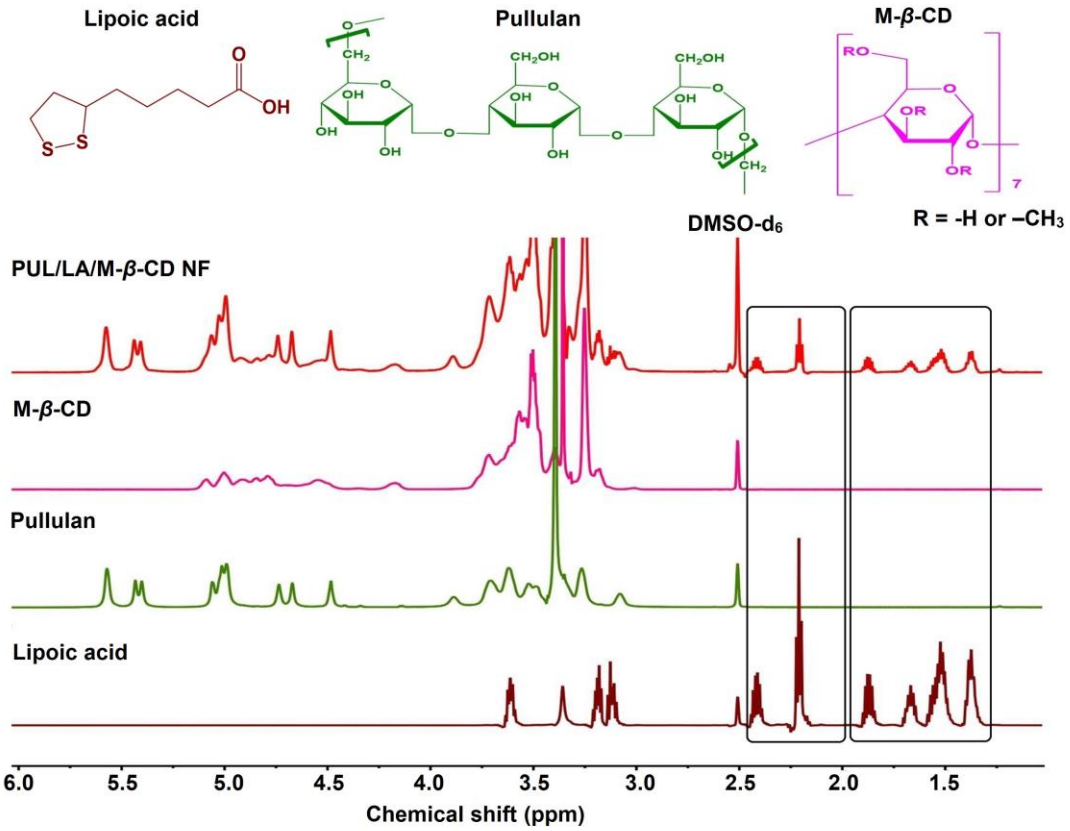

Figure 3: Proton NMR spectra of Lipoic acid (LA), Pullulan (PUL), Methyl-*β*-cyclodextrin (M-*β*-CD) and Pullulan/lipoic acid/M-*β*-CD nanofiber (PUL/LA/M-*β*-CD NF) in DMSO-d_6 solvent. Highlighted portion represents the characteristic peaks of LA observed in both LA and PUL/LA/M-*β*-CD NF, indicating the successful encapsulation and preservation of LA during electrospinning process.

Fourier transform infrared (FT-IR) spectroscopy analysis

The fourier transform infrared (FT-IR) spectra of LA, PUL, M-*β*-CD and PUL/LA/M-β-CD NF was performed to investigate the formation of inclusion complexes and possible molecular interactions between the guest molecules (LA) and the host molecules (M-*β*-CD) [17]. The FT-IR spectrum of LA displayed absorption bands at 1692.66 cm^{-1} and 2928.46 cm^{-1}, which corresponded to the stretching vibrations of the C=O bond and the O-H bond, respectively [2, 8]. The spectrum of M-*β*-CD exhibited a characteristic band in the range of 3400–3700 cm^{-1}, indicating the presence of free -OH groups [18]. While in case of PUL demonstrated a similar pattern to M-*β*-CD due to the presence of *α*(1→4) linked glucopyranose units. Notable peaks in the pullulan spectrum included O–H stretching (3414.12 cm^{-1}), C–H stretching (2929 cm^{-1}), H–O–H bending (1638.12 cm^{-1}), and C–O stretching (1200-1000 cm^{-1}) [19,20]. The FT-IR spectrum of PUL/LA/M-*β*-CD NF demonstrated shift in characteristic peaks of LA

(e.g., from 1708 cm^{-1} to 1809 cm^{-1}) and some peaks were masked because of M-*β*-CD and PUL with similar regions [8]. However, no additional peaks were observed in the NF spectra, indicating that no new chemical bonds were formed.

Differential scanning calorimetry (DSC) analysis

Differential scanning calorimetry (DSC) was used to further characterize the inclusion complex formation and encapsulation of LA inside nanofiber**.** The DSC thermogram of LA exhibited a sharp endothermic peak at ~ 64°C, representing its melting point and crystalline nature [8, 15]. Conversely, PUL and NFs displayed broad endothermic peaks in the range of 150-250°C and 150-200°C, respectively, indicative of dehydration. However, no such peaks were observed in the DSC thermograms of M-*β*-CD. In DSC thermograms of PUL/LA/M-*β*-CD NF, the melting peak of LA was not detected, suggesting complete inclusion complexation and encapsulation of LA within the NF.

Thermal gravimetric analysis (TGA)

The TGA thermograms depicted the thermal behavior of LA, PUL, M-*β*-CD, and PUL/LA/M-*β*-CD NF **(Figure 4c)**. The LA thermogram revealed a single-step degradation process, with 97% degradation of LA between 160-260 °C. In contrast, PUL, M-*β*-CD, and PUL/LA/M-*β*-CD NF exhibited a step-wise degradation pattern, starting with minor weight loss (%) below 100 °C, attributed to water evaporation. The main thermal degradation of M-*β*-CD (~ 85%) occurred between 300-388 °C, while PUL experienced its main degradation (~ 82%) between 270-340 °C. The TGA thermogram of PUL/LA/M-*β*-CD NF displayed weight losses in multiple steps. The primary weight loss, corresponding to the main degradation of the NF was observed between 250-300 °C (39% degradation) and 300-383 °C (up to 77% degradation). It was worth noting that the NF substantially enhanced the thermal stability of LA by increasing its complete degradation temperature from ~ 260 °C to 357 °C.

Powder X-ray diffraction (P-XRD) analysis

The inclusion complexation between LA and M-*β*-CD NF was confirmed by powder X-ray diffraction (P-XRD). The XRD spectra of LA, a crystalline molecule, showed distinct peaks at 23.8°, 24.46°, and 25.5° [8]. Both M-*β*-CD and PUL are amorphous, so their XRD patterns exhibited broad halos without significant diffraction peaks [18, 21].

The XRD pattern of PUL/LA/M-*β*-CD NF did not demonstrated any specific diffraction peaks corresponding to crystalline LA. This indicates that the LA molecules were in an inclusion complexed state with M-*β*-CD and successfully encapsulated in the NF.

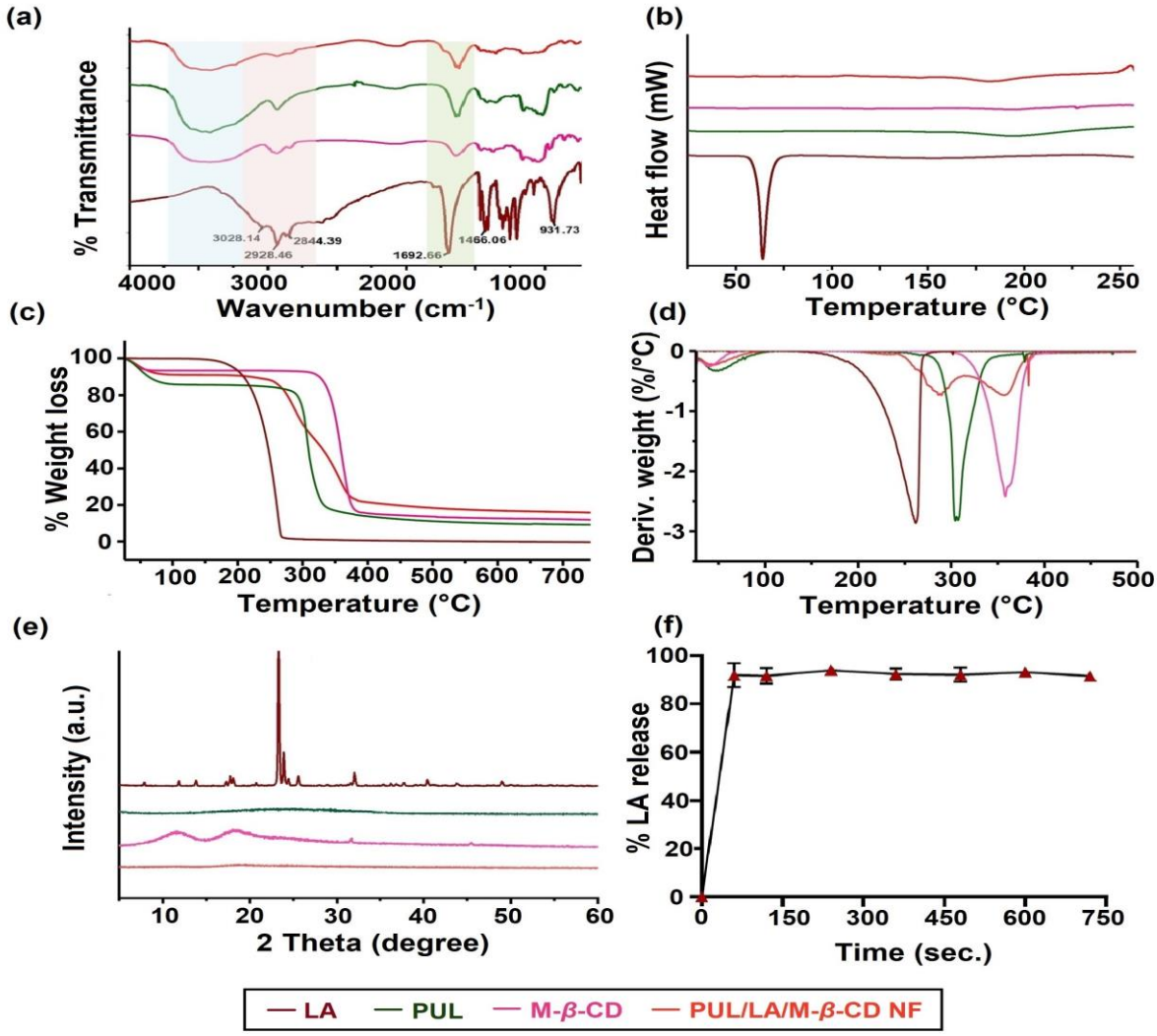

Figure 4: Structural characterization and release profile of PUL/LA/M-*β*-CD NF. (a) FT-IR spectra, (b) DSC thermogram, (d) TGA thermogram, (d) derivative weight (%) loss curve and (e) XRD diffractogram of LA (brown), PUL (green), M-*β*-CD (magenta) and PUL/LA/M-*β*-CD NF (red). Highlighted portions in FT-IR spectra represent the masking, shifting and broadening of LA bands after inclusion complex and nanofiber formation. (f) *In vitro* time dependent release profile of LA from PUL/LA/M-*β*-CD NF expressed in cumulative % release over the period of 12 minutes.

In vitro time dependent release, disintegration and dissolution behaviour of NF

The release of LA from PUL/LA/M-*β*-CD NF was studied over time, and the results are presented as a cumulative percentage release. The study demonstrated that

PUL/LA/M-*β*-CD NF dissolves instantly upon contact with water, leading to ~ 94% of release from the NF matrix within 60 seconds. The fast release profile of LA can be attributed to the unique characteristics of the inclusion complex formation, high surface area, uniform NF size, and porosity [8].

Furthermore, the dissolution behaviour of PUL/LA/M-*β*-CD NF was compared with native LA and blank NF. The study demonstrated PUL/LA/M-*β*-CD NF dissolved instantly (within 30 second) due to the high water solubility of CD and PUL. In contrast, LA remained undissolved even after 1 minute, indicating poor dissolution profile of LA attributed to its crystalline nature [8].

The disintegration characteristics of both the blank and PUL/LA/M-*β*-CD NF were assessed in a simulated oral environment using filter paper saturated with artificial saliva. Both the blank and PUL/LA/M-*β*-CD NF exhibited rapid disintegration within 2 seconds upon contact with artificial saliva. The NF's high surface area and porosity facilitate the easy penetration of liquids, contributing to fast disintegration and dissolution of the NF [19]. To summarize, the nano size fibrous structure of PUL/LA/M-*β*-CD NF ensures the effortless entry of saliva into the mouth. Furthermore, the formation of inclusion complexes between LA and M-*β*-CD, along with the high water solubility of modified CD, promotes the instantaneous release of LA through rapid dissolution.

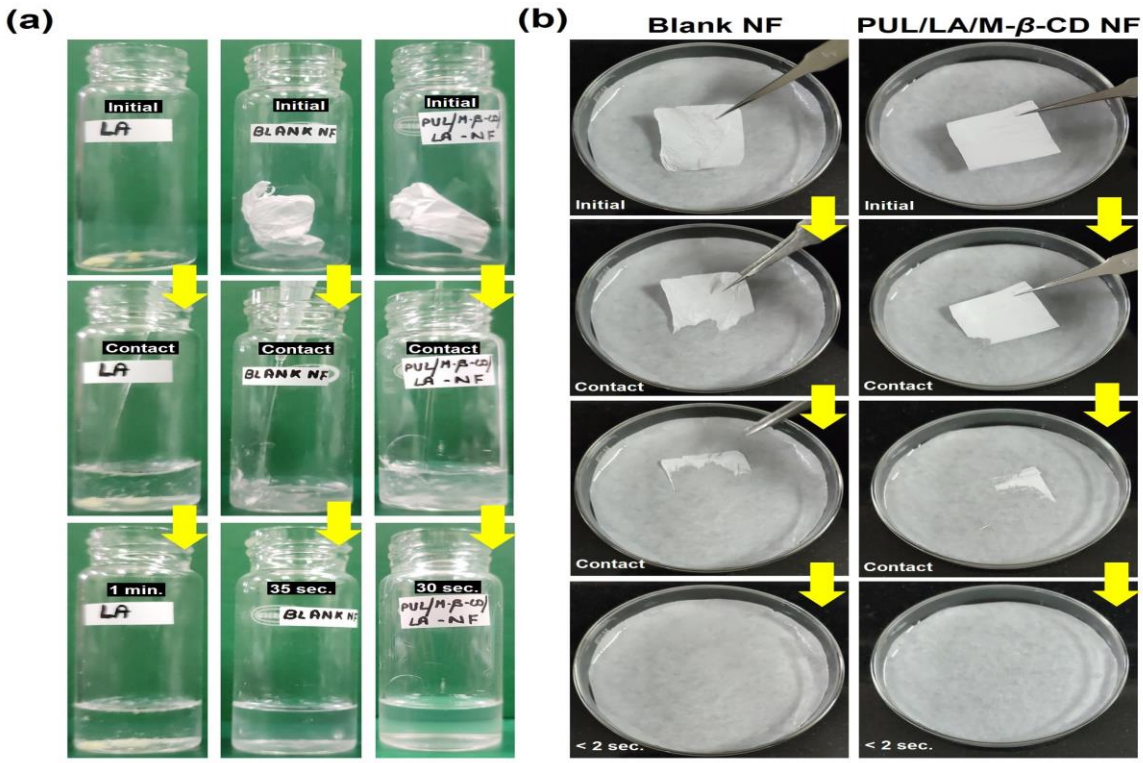

Figure 5: Dissolution and disintegration behaviour of PUL/LA/M-*β*-CD NF. (a) Dissolution behaviour of PUL/LA/M-*β*-CD NF in comparison to blank NF and native LA in 5 mL distilled water. (b) Disintegration behaviour of PUL/LA/M-*β*-CD NF in comparison to blank NF in artificial saliva.

In vitro evaluation of anti-inflammatory activity of PUL/LA/M-*β*-CD nanofibers

Effect of PUL/LA/M-*β*-CD NF on viability of RAW 264.7 macrophage cells

The cytocompatibility of developed PUL/LA/M-*β*-CD NF on 264.7 macrophage cells was evaluated using MTT cell viability assay. The cell viability results demonstrated that PUL/LA/M-*β*-CD NF and LA has negligible effect on the viability of RAW macrophage cells and the induction of LPS (1 µg/mL) did not influence the cell viability. The effect of blank nanofibers on RAW macrophage cells were also assessed and exhibited negligible effect on cell viability upto 500 µg/mL**.** The morphological changes in the RAW 264.7 macrophages cells were also examined in the control, LPS, LA and PUL/LA/M-*β*-CD NF-treated groups. The RAW 264.7 macrophages under normal conditions appeared small, round with smooth surfaces and have homogeneous sizes [22]. The exposure of LA and PUL/LA/M-*β*-CD NF at different concentrations (100 µM, 250 µM and 500 µM) did not impose any significant effects on the cell morphology. However, exposure to LPS (24 h) resulted in notable morphological changes in the macrophages, such as irregular polygonal shape,

increased cell volume, increased quantity of intracellular granular vesicles, high vacuolation, formation of thin and long dendritic pseudopodia on the cell surface. These modifications demonstrated that LPS significantly induced inflammation in the RAW 264.7 macrophages [23]. Interestingly, the administration of PUL/LA/M-*β*-CD NF exhibited protection and prevention of LPS-induced changes in macrophage morphology in a concentration-dependent manner. PUL/LA/M-*β*-CD NF (500 µM equivalent to LA) demonstrated notable protective effect on the morphology of RAW 264.7 macrophages in comparison to LPS as well as LA.

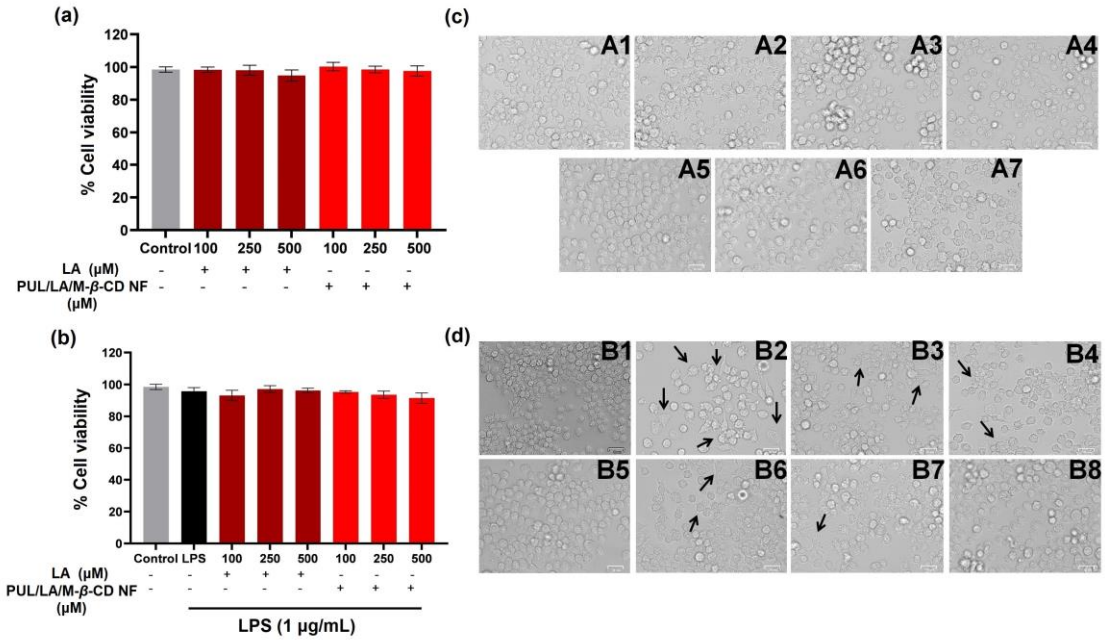

Figure 6: Effect of PUL/LA/M-*β*-CD NF on cell viability of RAW 264.7 macrophage cells in presence and absence of LPS induction. (a) & (b) cell viability graph of RAW 264.7 macrophage after 24 h treatment with LA and PUL/LA/M-*β*-CD NF at different concentration (100, 250 and 500 µM) without and with LPS, respectively. (c) & (d) microscopic images of RAW 264.7 macrophage cells representing morphological characteristics before (c) and after LPS induction (black headed arrows, d [B2]). PUL/LA/M-*β*-CD NF demonstrated concentration-dependent retention of normal RAW 264.7 macrophage morphology even after LPS induction (B6, 7 &8). Images were captured using fluorescent microscope (ZOE™ Fluorescent Cell Imager, Bio-Rad). White line represents 25 µm scale bar.

Effect of PUL/LA/M-*β*-CD NF on LPS induced NO production in RAW 264.7 macrophage cells

NO, a pro-inflammatory mediator released by macrophages, is considered a key marker of inflammation and is produced by iNOS in macrophages [24]. Its production is

a part of the innate immune response in mammals and can indicate the progression of inflammation following exposure to LPS. However, excessive production of NO by triggered macrophages is associated with the development of inflammation-related disorders [25]. Therefore, ameliorated effect of PUL/LA/M-*β*-CD NF on NO production in RAW 264.7 macrophages was evaluated using Griess reagent. The results demonstrated significantly higher NO production in LPS group as compared to control group. However, PUL/LA/M-*β*-CD NF demonstrated a significant concentration-dependent reduction in NO production compared to both LPS group as well as LA groups.

Effect of PUL/LA/M-*β*-CD NF on LPS induced ROS generation in RAW 264.7 macrophage cells

Oxidative stress and inflammatory response are commonly present in various diseases, and both contribute to and accelerate the progression of the illness. Reactive oxygen species (ROS) plays a role in inflammation in two ways. Firstly, it acts as a redox signal that regulates the duration of inflammation. Additionally, the accumulation of ROS-damaged tissue further exacerbates the production of inflammatory vesicles [55]. Moreover, ROS can trigger the NF-κB pathways, leading to the release of pro-inflammatory cytokines [26]. Therefore, the study aimed to evaluate the improved effect of PUL/LA/M-*β*-CD NF on ROS generation in RAW 264.7 macrophages using DCF-DA dye. The results demonstrated significant increase in ROS generation in RAW 264.7 macrophages upon induction of LPS as compared to the control group. However, PUL/LA/M-*β*-CD NF demonstrated a concentration-dependent decrease in ROS generation, which was more pronounced compared to both the LPS group and the LA groups. Microscopic images of ROS visualized using DCF-DA fluorescent dye also demonstrated the efficacy of PUL/LA/M-*β*-CD NF in significantly decreasing the ROS generation as compared to native LA.

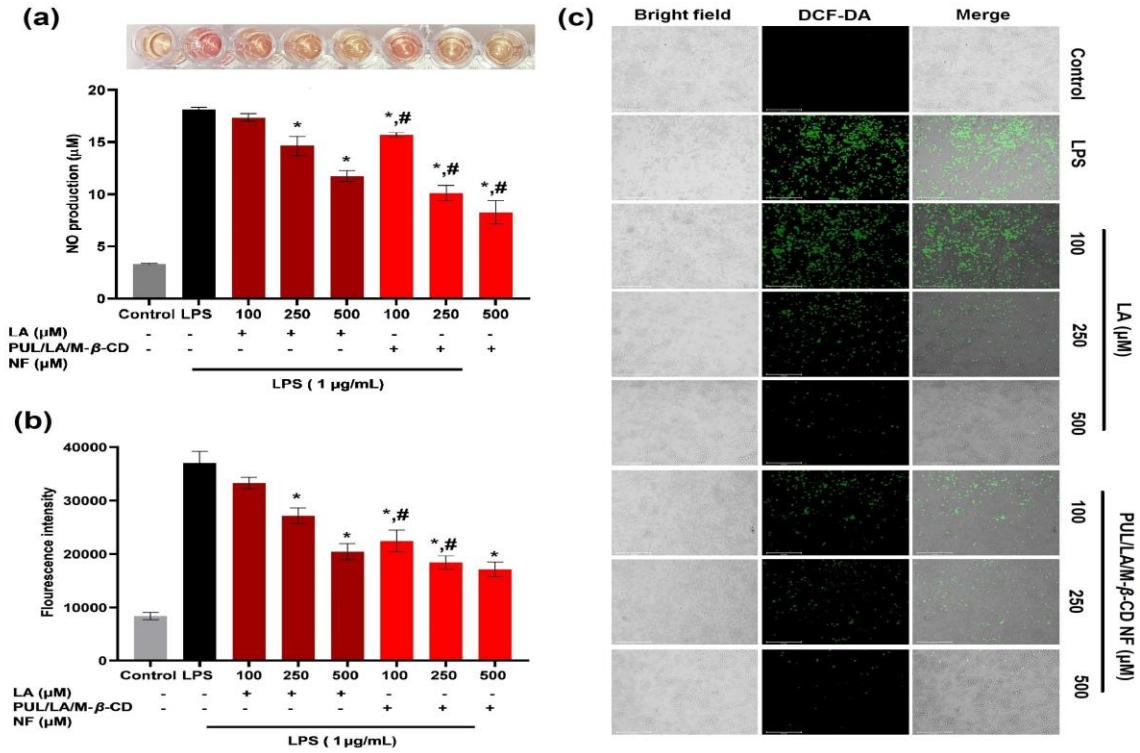

Figure 7: Effect of PUL/LA/M-*β*-CD NF on LPS induced NO and ROS production in RAW 264.7 macrophage cells after its 24 h treatment followed by 24 h LPS induction. (a) Graph of NO production in RAW 264.7 macrophage after 24 h treatment with LA and PUL/LA/M-*β*-CD NF at different concentrations (100, 250 and 500 µM) followed by LPS induction. PUL/LA/M-*β*-CD NF demonstrated concentration dependent ameliorated effect on LPS induced NO production. The amount of NO production was measured by Griess reagent. (b) Graph of ROS generation in RAW 264.7 macrophage after 24 h treatment with LA and PUL/LA/M-*β*-CD NF at different concentrations followed by LPS induction. Generation of ROS was evaluated by using DCF-DA fluorescent dye and change in fluorescence intensity was plotted as graph. (c) Microscopic images of ROS generation, visualized by using DCF-DA green fluorescent dye. Images were captured using fluorescent microscope (EVOS FL Auto 2 Cell Imaging System, Invitrogen). * $p<0.05$ indicates significant difference in the mean value from LPS group. # $p<0.05$ indicates significant difference in the mean value of PUL/LA/M-*β*-CD NF from LA group (with respective concentrations).

Suppressive effect of PUL/LA/M-*β*-CD NF on mRNA level of pro-inflammatory enzymes/cytokines

The macrophages serve as the initial defence against infections and play a vital role in protecting the body from various infections [24]. However, excessive activation of macrophages can contribute to the development of inflammatory disorders by generating abundance quantity of pro-inflammatory enzyme and cytokines. This abnormal activation is often triggered by exposure to LPS, a component found in the

outer membrane of gram^{-ve} bacteria [27]. LPS is commonly used to study the inflammatory responses in RAW 264.7 macrophages. These macrophages, when exposed to LPS, have been extensively observed to increase the production pro-inflammatory enzymes like iNOS and COX-2 [22, 28]. Both iNOS and COX-2 are crucial enzymes responsible for generating two major inflammatory mediators: NO and PGE2, respectively. In addition, activated macrophages release significant levels of pro-inflammatory cytokines such as TNF-*α*, IL-1*β*, and IL-6. These can influence a complex signalling network involved in inflammation. For instance, TNF-*α* and IL-1*β* promote neutrophil accumulation and the release of other cytokines, initiating and perpetuating the inflammatory response. On the other hand, IL-6 helps in maintaining tissue balance and regulates the extent of the inflammatory responses [22].

LA possesses promising anti-inflammatory activities by suppressing the overexcited expressions of pro-inflammatory enzymes and cytokines [29]. Therefore, the ameliorated effect of PUL/LA/M-*β*-CD NF (nanofibers) on downregulating the mRNA levels of pro-inflammatory enzymes (iNOS and COX-2) and cytokines (TNF-*α*, IL-1*β*, and IL-6) was determined by qRT-PCR. The results of qRT-PCR demonstrated that PUL/LA/M-*β*-CD NF significantly downregulates the mRNA levels of iNOS, COX-2, TNF-*α*, IL-1*β*, and IL-6 compared to both LPS and LA (250 µM) group.

Suppressive effect of PUL/LA/M-*β*-CD NF on protein expression of COX-2 in RAW 264.7 macrophage cells

The ameliorated effect of PUL/LA/M-*β*-CD NF on protein expression of COX-2 was also evaluated using western blotting. The results of COX-2 western blotting demonstrated that PUL/LA/M-β-CD NF treatment significantly suppressed the protein expression of COX-2 in RAW 264.7 macrophages as compared to the LPS and LA group (250 µM concentration). Moreover, RAW 264.7 macrophages of control group presented negligible expression of COX-2 protein which is usually observed in LPS untreated cells whereas, a significant upregulation of COX-2 protein expression was observed in LPS group [30].

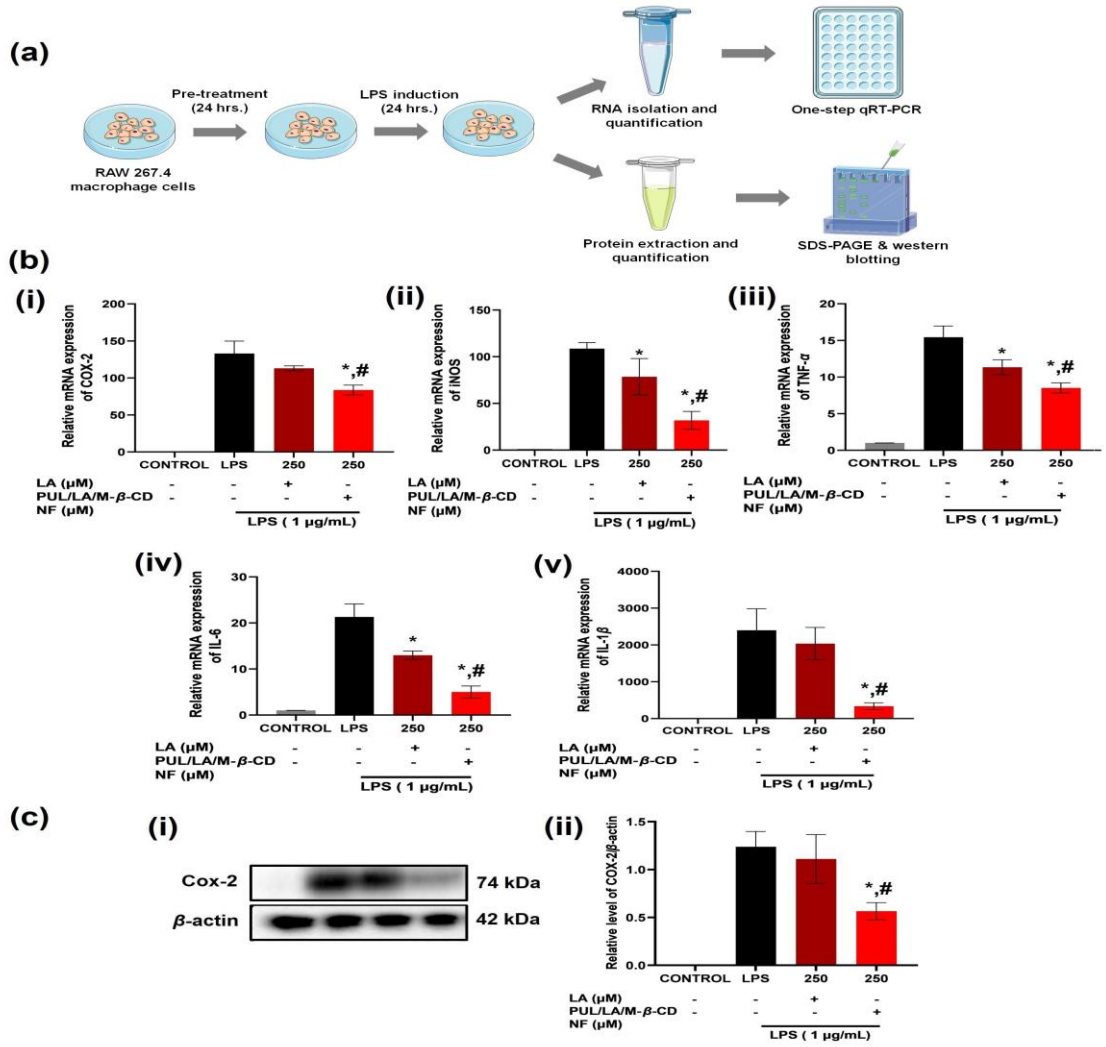

Figure 8: (a) Schematic representation of methodology followed for the treatment, protein and RNA isolation from LPS induced RAW264.7 macrophage cells.(b) & (c) Suppressive effect of PUL/LA/M-*β*-CD NF on mRNA level of pro-inflammatory enzymes/cytokines and protein levels of COX-2 in LPS induced RAW 264.7 macrophage cells.mRNA levels of iNOS, COX-2, TNF-*α*, IL-6 and IL-1*β* was analysed by qRT-PCR in cells treated with LA and PUL/LA/M-*β*-CD NF (250 µM equivalent to LA) for 24 h followed by induction of LPS (1 µg/mL) for another 24 h. Protein expression of COX-2 was analysed by western blotting in cells treated with LA and PUL/LA/M-*β*-CD NF (250 µM equivalent to LA) for 24 h followed by induction of LPS (1 µg/mL) for another 24 h.* $p<0.05$ indicates significant difference in the mean value from LPS group. # $p<0.05$ indicates significant difference in the mean value of PUL/LA/M-*β*-CD NF from LA group (with respective concentrations).

Inhibitory effect of PUL/LA/M-*β*-CD NF on LPS-stimulated nuclear translocation of NF-κB in RAW264.7 macrophage cells

The iNOS and COX-2 matrix proteinases are crucial pro-inflammatory enzymes, and their gene expression is regulated by downstream signalling of NF-κB. NF-κB acts as

a transcription factor and plays a vital role in managing the transcription of various inflammation-related genes. Downregulation of NF-κB leads to decrement in generation of pro-inflammatory cytokines such as TNF-*α*, IL-6, and IL-1*β* [11, 24].

Based on these facts, we further assessed the ability of NF to suppress the nuclear translocation of NF-κB. The results demonstrated that PUL/LA/M-*β*-CD NF (at 250 µM equivalent to LA**)** significantly suppresses the nuclear translocation of NF-κB in comparison to LA.

Overall, PUL/LA/M-*β*-CD NF exhibited an improved anti-inflammatory activity compared to LA by suppressing LPS-induced NO production, ROS generation, downregulation of pro-inflammatory enzymes, cytokines and inhibition of NF-κB nuclear translocation in RAW 264.7 macrophage cells.

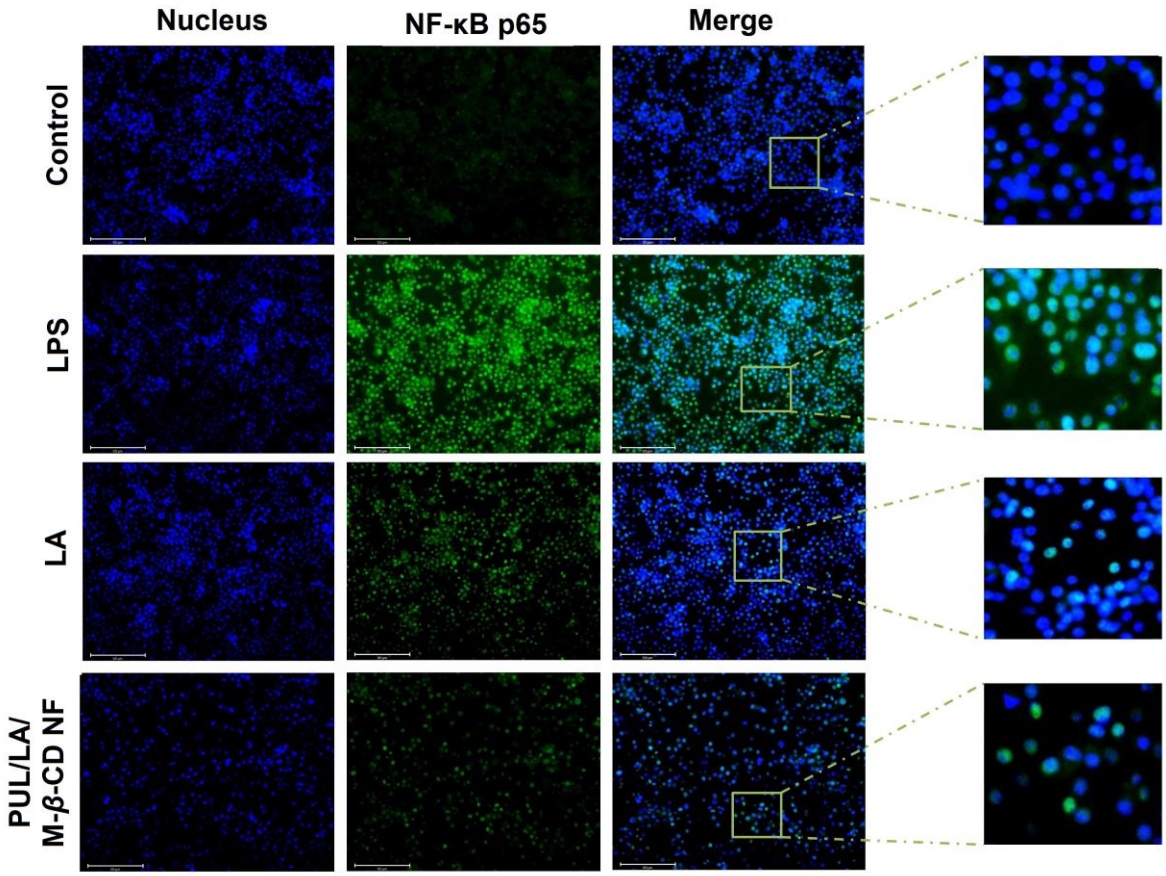

Figure 9: Inhibitory effect of PUL/LA/M-*β*-CD NF on LPS-stimulated nuclear translocation of NF-κB in RAW264.7 macrophage cells analysed by fluorescent microscopy. Macrophages were immunostained by Alexa Fluor 488 for NF-κB and DAPI for nuclei staining. Images were captured using fluorescent microscope (EVOS FL Auto 2 Cell Imaging System, Invitrogen). White line represents 125 µm scale bar.

5. Statistics analysis

The results were displayed as the mean and standard deviation (SD) for three separate values (n = 3). One-way analysis of variance with a Tukey's post hoc test was used to determine the significant difference between the means of each group using the graph pad prism software 9 (GraphPad Software Inc, CA, USA) at significance level of $p < 0.05$.

6. Impact of the research in the advancement of knowledge or benefit to mankind

Nanofiber-based oral thin films represent a remarkable advancement in the field of drug delivery and medical technology, offering numerous benefits and a potential for significant social impact. These innovative films are ultra-thin layers that contain nanoscale fibers, usually composed of biocompatible polymers, and are designed to be placed on the tongue or buccal mucosa (inner cheek) for rapid drug absorption into the bloodstream. The significance of these nanofiber-based oral thin films lies in their enhanced therapeutic efficacy, improved patient compliance, and broader societal implications. Rapid drug delivery and improved patient compliance may result in quicker recovery times and better disease management, ultimately improving the quality of life for patients. Furthermore, these films could aid in expanding access to healthcare in underserved or remote areas.

Current study is the perfect example of sustainable and green method for the development of such a delivery system with ameliorated therapeutic potential and high patient compliance. Moreover, study has opened new avenues in terms of sustainable approach for production of nanofibers as well as its mechanistic insight for anti-inflammatory activity. Additionally, the simplicity of administration, reduced need for specialized medical personnel, and potential for self-administration could make these more accessible to populations with limited healthcare infrastructure.

7. References

(1) Lv, S.-y.; He, S.; Ling, X.-l.; Wang, Y.-q.; Huang, C.; Long, J.-r.; Wang, J.-q.; Qin, Y.; Wei, H.; Yu, C.-Y. Review of lipoic acid: from a clinical therapeutic agent to various emerging biomaterials. *International Journal of Pharmaceutics* **2022**, 122201.

(2) Ruchika; Kumari, S.; Dhiman, P.; Singh, D.; Saneja, A. R-α-Lipoic Acid Conjugated to d-α-Tocopherol Polyethylene Glycol 1000 Succinate: Synthesis, Characterization, and Effect on Antiseizure Activity. *Journal of Agricultural and Food Chemistry* **2022**, *70* (25), 7674-7682.

(3) Tibullo, D.; Li Volti, G.; Giallongo, C.; Grasso, S.; Tomassoni, D.; Anfuso, C. D.; Lupo, G.; Amenta, F.; Avola, R.; Bramanti, V. Biochemical and clinical relevance of alpha lipoic acid: antioxidant and anti-inflammatory activity, molecular pathways and therapeutic potential. *Inflammation Research* **2017**, *66*, 947-959.

(4) Kaur, D.; Behl, T.; Sehgal, A.; Singh, S.; Sharma, N.; Chigurupati, S.; Alhowail, A.; Abdeen, A.; Ibrahim, S. F.; Vargas-De-La-Cruz, C. Decrypting the potential role of α-lipoic acid in Alzheimer's disease. *Life Sciences* **2021**, *284*, 119899.

(5) Altunina, N. V.; Lizogub, V. G.; Bondarchuk, O. M. Alpha-lipoic acid as a means of influence on systemic inflammation in type 2 diabetes mellitus patients with prior myocardial infarction. *Journal of medicine and life* **2020**, *13* (1), 32.

(6) Khan, N.; Bhardwaj, V. K.; Purohit, R.; Saneja, A. Deciphering the interactions of genistein with β-cyclodextrin derivatives through experimental and microsecond timescale umbrella sampling simulations. *Journal of Molecular Liquids* **2023**, *374*, 121295.

(7) Higuchi, T.; Connors, K. Adv anal chem instrum. *Phase-solubility techniques* **1965**, *4*, 117-212.

(8) Celebioglu, A.; Uyar, T. Encapsulation and stabilization of α-lipoic acid in cyclodextrin inclusion complex electrospun nanofibers: Antioxidant and fast-dissolving α-lipoic acid/cyclodextrin nanofibrous webs. *Journal of agricultural and food chemistry* **2019**, *67* (47), 13093-13107.

(9) Celebioglu, A.; Wang, N.; Kilic, M. E.; Durgun, E.; Uyar, T. Orally fast disintegrating cyclodextrin/prednisolone inclusion-complex nanofibrous webs for potential steroid medications. *Molecular Pharmaceutics* **2021**, *18* (12), 4486-4500.

(10) Liu, C.; Lu, R.; Jia, M.; Xiao, X.; Chen, Y.; Li, P.; Zhang, S. Biological Glue from Only Lipoic Acid for Scarless Wound Healing by Anti-inflammation and TGF-β Regulation. *Chemistry of Materials* **2023**, *35* (6), 2588-2599.

(11) Park, J.-Y.; Chung, T.-W.; Jeong, Y.-J.; Kwak, C.-H.; Ha, S.-H.; Kwon, K.-M.; Abekura, F.; Cho, S.-H.; Lee, Y.-C.; Ha, K.-T. Ascofuranone inhibits lipopolysaccharide–induced inflammatory response via NF-kappaB and AP-1, p-

ERK, TNF-α, IL-6 and IL-1β in RAW 264.7 macrophages. *PLoS One* **2017**, *12* (2), e0171322.

(12) Zhang, J.; Zhang, M.; Huo, X.-K.; Ning, J.; Yu, Z.-L.; Morisseau, C.; Sun, C.-P.; Hammock, B. D.; Ma, X.-C. Macrophage inactivation by small molecule wedelolactone via targeting sEH for the treatment of LPS-induced acute lung injury. *ACS Central Science* **2023**, *9* (3), 440-456.

(13) He, J.-W.; Guo, P.; Yang, L.; He, J.-W. Anti-inflammatory constituents isolated from the flowers of Hosta plantaginea via suppression of the NF-κB signaling pathway in LPS-stimulated RAW 264.7 macrophages. *RSC advances* **2023**, *13* (11), 7179-7184.

(14) Zhang, M.; Wei, X.; Xu, X.; Jin, Z.; Wang, J. Synthesis and characterization of water-soluble β-cyclodextrin polymers via thiol-maleimide 'click'chemistry. *European Polymer Journal* **2020**, *128*, 109603.

(15) Maeda, H.; Onodera, T.; Nakayama, H. Inclusion complex of α-lipoic acid and modified cyclodextrins. *Journal of Inclusion Phenomena and Macrocyclic Chemistry* **2010**, *68*, 201-206.

(16) Poudel, D.; Swilley-Sanchez, S.; O'keefe, S.; Matson, J.; Long, T.; Fernández-Fraguas, C. Novel electrospun pullulan fibers incorporating hydroxypropyl-β-cyclodextrin: morphology and relation with rheological properties. *Polymers* **2020**, *12* (11), 2558.

(17) Wang, L.; Li, S.; Tang, P.; Yan, J.; Xu, K.; Li, H. Characterization and evaluation of synthetic riluzole with β-cyclodextrin and 2, 6-di-O-methyl-β-cyclodextrin inclusion complexes. *Carbohydrate polymers* **2015**, *129*, 9-16.

(18) de Freitas, M. R.; Rolim, L. A.; Soares, M. F. d. L. R.; Rolim-Neto, P. J.; de Albuquerque, M. M.; Soares-Sobrinho, J. L. Inclusion complex of methyl-β-cyclodextrin and olanzapine as potential drug delivery system for schizophrenia. *Carbohydrate polymers* **2012**, *89* (4), 1095-1100.

(19) Ertan, K.; Celebioglu, A.; Chowdhury, R.; Sumnu, G.; Sahin, S.; Altier, C.; Uyar, T. Carvacrol/cyclodextrin inclusion complex loaded gelatin/pullulan nanofibers for active food packaging applications. *Food Hydrocolloids* **2023**, *142*, 108864.

(20) Hsiung, E.; Celebioglu, A.; Kilic, M. E.; Durgun, E.; Uyar, T. Fast-Disintegrating Nanofibrous Web of Pullulan/Griseofulvin–Cyclodextrin Inclusion Complexes. *Molecular Pharmaceutics* **2023**, *20* (5), 2624-2633.

(21) Qin, Z.; Zou, Y.; Zhang, Y.; Wang, P.; Zhang, H. Electrospun pullulan nanofiber loading zanthoxylum bungeanum essential oil/β-cyclodextrin inclusion complexes for active packaging. *International Journal of Biological Macromolecules* **2022**, *210*, 465-474.

(22) Wang, G.; Zhan, Q.; Wu, H. Suppression of lipopolysaccharide-induced activation of RAW 264.7 macrophages by Se-methylseleno-l-cysteine. *International Immunopharmacology* **2020**, *89*, 107040.

(23) Liu, Z.; Zhang, J.; Jiang, P.; Yin, Z.; Liu, Y.; Liu, Y.; Wang, X.; Hu, L.; Xu, Y.; Liu, W. Paeoniflorin inhibits the macrophage-related rosacea-like inflammatory reaction through the suppressor of cytokine signaling 3-apoptosis signal-regulating kinase 1-p38 pathway. *Medicine* **2021**, *100* (3).

(24) Nie, Y.; Wang, Z.; Chai, G.; Xiong, Y.; Li, B.; Zhang, H.; Xin, R.; Qian, X.; Tang, Z.; Wu, J. Dehydrocostus lactone suppresses LPS-induced acute lung injury and macrophage activation through NF-κB signaling pathway mediated by p38 MAPK and Akt. *Molecules* **2019**, *24* (8), 1510.

(25) Kim, C. H.; Hwang, B. S.; Hwang, Y.; Oh, Y. T.; Jeong, J.-W. Evaluation of antioxidant and antiinflammatory activity of ethanolic extracts of Polygonum senticosum in lipopolysaccharide-induced RAW 264.7 macrophages. *Journal of Laboratory Medicine* **2022**, *46* (1), 51-59. Bai, M.-Y.; Hu, Y.-M. Development of alpha-lipoic acid encapsulated chitosan monodispersed particles using an electrospray system: synthesis, characterisations and anti-inflammatory evaluations. *Journal of Microencapsulation* **2014**, *31* (4), 373-381. Kiemer, A. K.; Müller, C.; Vollmar, A. M. Inhibition of LPS-induced nitric oxide and TNF-α production by α-lipoic acid in rat Kupffer cells and in RAW 264.7 murine macrophages. *Immunology and cell biology* **2002**, *80* (6), 550-557. DeMarco, V. G.; Scumpia, P. O.; Bosanquet, J. P.; Skimming, J. W. α-lipoic acid inhibits endotoxin-stimulated expression of iNOS and nitric oxide independent of the heat shock response in RAW 264.7 cells. *Free radical research* **2004**, *38* (7), 675-682. Aly, H. A.; Lightfoot, D. A.; El-Shemy, H. A. Modulatory role of lipoic acid on lipopolysaccharide-induced oxidative stress in adult rat Sertoli cells in vitro. *Chemico-biological interactions* **2009**, *182* (2-3), 112-118.

(26) Szulc-Kielbik, I.; Kielbik, M.; Klink, M. Ferulic acid but not alpha-lipoic acid effectively protects THP-1-derived macrophages from oxidant and pro-inflammatory response to LPS. *Immunopharmacology and Immunotoxicology* **2017**, *39* (6), 330-337. Xia, X.; Su, C.; Fu, J.; Zhang, P.; Jiang, X.; Xu, D.; Hu, L.; Song, E.; Song, Y.

Role of α-lipoic acid in LPS/d-GalN induced fulminant hepatic failure in mice: studies on oxidative stress, inflammation and apoptosis. *International immunopharmacology* **2014**, *22* (2), 293-302. Wang, Y.; Zheng, Y.; Qi, B.; Liu, Y.; Cheng, X.; Feng, J.; Gao, W.; Li, T. α-Lipoic acid alleviates myocardial injury and induces M2b macrophage polarization after myocardial infarction via HMGB1/NF-kB signaling pathway. *International Immunopharmacology* **2023**, *121*, 110435.

(27) Shi, H.; Wang, X.-L.; Quan, H.-F.; Yan, L.; Pei, X.-Y.; Wang, R.; Peng, X.-D. Effects of betaine on LPS-stimulated activation of microglial M1/M2 phenotypes by suppressing TLR4/NF-κB pathways in N9 cells. *Molecules* **2019**, *24* (2), 367.

(28) Xiong, H.; Cheng, Y.; Zhang, X.; Zhang, X. Effects of taraxasterol on iNOS and COX-2 expression in LPS-induced RAW 264.7 macrophages. *Journal of ethnopharmacology* **2014**, *155* (1), 753-757.

(29) Jing, P.; Luo, Y.; Chen, Y.; Tan, J.; Liao, C.; Zhang, S. Aspirin-Loaded Cross-Linked Lipoic Acid Nanodrug Prevents Postoperative Tumor Recurrence by Residual Cancer Cell Killing and Inflammatory Microenvironment Improvement. *Bioconjugate Chemistry* **2023**, *34* (2), 366-376.

(30) Kwon, D.-J.; Ju, S. M.; Youn, G. S.; Choi, S. Y.; Park, J. Suppression of iNOS and COX-2 expression by flavokawain A via blockade of NF-κB and AP-1 activation in RAW 264.7 macrophages. *Food and chemical toxicology* **2013**, *58*, 479-486. Ninomiya, Y.; Tanuma, S.-i.; Tsukimoto, M. Differences in the effects of four TRPV1 channel antagonists on lipopolysaccharide-induced cytokine production and COX-2 expression in murine macrophages. *Biochemical and biophysical research communications* **2017**, *484* (3), 668-674.